

# Tunable megawatt-scale sub-20 fs visible pulses from a fiber laser source

MOHAMMED SABBAH<sup>1</sup>, ROBBIE MEARS<sup>2</sup>, LEAH R. MURPHY<sup>1</sup>, KERRIANNE HARRINGTON<sup>2</sup>, JAMES M. STONE<sup>2</sup>, TIM A. BIRKS<sup>2</sup>, AND JOHN C. TRAVERS<sup>1,\*</sup>

<sup>1</sup>School of Engineering and Physical Sciences, Heriot-Watt University, Edinburgh, United Kingdom

<sup>2</sup>Centre for Photonics and Photonic Materials, Department of Physics, University of Bath, Claverton Down, Bath, BA2 7AY, United Kingdom

\*j.travers@hw.ac.uk

Compiled February 4, 2025

**Tunable ultrashort laser pulses across the near-ultraviolet to near-infrared with high peak power are crucial for wide-ranging applications in science and industry. Resonant dispersive-wave emission in gas-filled hollow-core fibers is a well-established technique for generating tunable ultrashort pulses from the vacuum ultraviolet to the near-infrared. However, previous demonstrations have relied on complex and expensive laser systems to provide the necessary energetic ultrashort pump pulses. Recent advances in fiber laser technology, particularly gain-managed nonlinear amplification, offer a promising alternative pump source. In this work, we combine gain-managed nonlinear amplification with resonant dispersive-wave emission to demonstrate a compact and tunable source of sub-20 fs pulses at 4.8 MHz. We achieve a tunable output spanning from 400 nm to beyond 700 nm, with energy up to 39 nJ, pulse duration down to 13 fs, and peak power exceeding 2 MW. This compact and efficient laser source opens new avenues for deploying resonant dispersive-wave-based technologies for broader scientific and industrial applications.**

<http://dx.doi.org/10.1364/ao.XX.XXXXXX>

Tunable ultrafast laser pulse sources with high peak power are widely exploited for applications in the biological and chemical sciences, such as multiphoton imaging and microscopy, and ultrafast spectroscopy [1–3]. The most common sources of such pulses in the visible and near-infrared region are tunable Ti:sapphire oscillators, optical parametric amplifiers, or filtered supercontinuum sources [2]. All of these are complex and come with one or more disadvantages in terms of cost, size, complexity, or performance. Although Ti:sapphire oscillators can produce short pulses down to 5 fs [4], scaling to high energy usually produces a significantly longer pulse duration ( $\sim 100$  fs). Widely-tunable Ti:sapphire oscillators are the work-horse laser system in multiphoton imaging, but their tunability is naturally limited from  $\sim 680$  nm to  $\sim 1080$  nm, without further nonlinear conversion stages that further increase complexity and reduce efficiency. Alternatively, optical parametric amplifiers can produce very short pulses with high energy, and can incorporate second or third harmonic pump stages to tune across the visible and near-infrared regions [5, 6]. However, they usually require high-energy amplified pump lasers, which makes them com-

plicated and expensive and forces them to operate at a relatively low repetition rate. Filtered supercontinuum sources are a much simpler route to rapid tunability and high average power, but they usually have long pulse duration, low pulse energy, and peak power, and often lack temporal coherence, prohibiting some applications [7].

Resonant dispersive-wave (RDW) generation in hollow-core fibers has been shown to be an excellent technique for generating tunable ultrashort pulses from the vacuum ultraviolet to the near-infrared [8–13]. The RDW generation process is a result of phase matching between a pump soliton and a linear wave in the presence of high-order dispersion [8, 14]. The duration of the generated RDW pulse can be as short as a few femtoseconds [15, 16]. To avoid modulation instability dynamics and produce high-quality and coherent pulses, the pump soliton order should be  $< 16$  [17], which usually requires short pump pulses of  $\sim 50$  fs or less, and moderately high energy in gas-filled fibers. By making use of the low guidance loss of antiresonant fibers, even for small core diameters, pump energy at the few to sub microjoule level is required. As a result, RDW generation is usually pumped with amplified Ti:sapphire or ytterbium (Yb) laser systems. While Ti:sapphire systems can produce high energy and short pulses (sub-40 fs), sufficient to drive RDW generation directly [8–10], Yb laser systems usually produce longer pulses  $\sim 200$  fs, requiring an additional temporal compression stage before RDW generation [11, 12]. Although RDW emission can be achieved with pump energies as low as 20 nJ after careful optimization in very small core fibers [18], this inherently results in low-energy tunable RDW pulses, thereby limiting their suitability for nonlinear applications that require high peak power.

Recent advances in fiber lasers and amplifiers have enabled the generation of sub-50 fs pulses with microjoule level energy with a simple architecture [19–21]. In particular, the recently developed gain-managed nonlinear amplification (GMNA) regime presents a promising approach due to its straightforward design, which eliminates the need for pre-chirping [22]. The GMNA approach is essentially an over-extended self-similar nonlinear amplifier [23]. A narrowband, low-energy seed pulse is introduced into the codirectionally-pumped gain fiber, where the interaction of spectral broadening with gain dynamics produces a broadband spectrum with an almost linear chirp. The resulting pulse can be compressed close to its transform-limited duration using a simple grating pair [24–26].

In this work, we combine a GMNA pump source with RDW emission in gas-filled hollow-core antiresonant fibers to demonstrate an ultrafast pulse source tunable across the near-ultraviolet to the near-

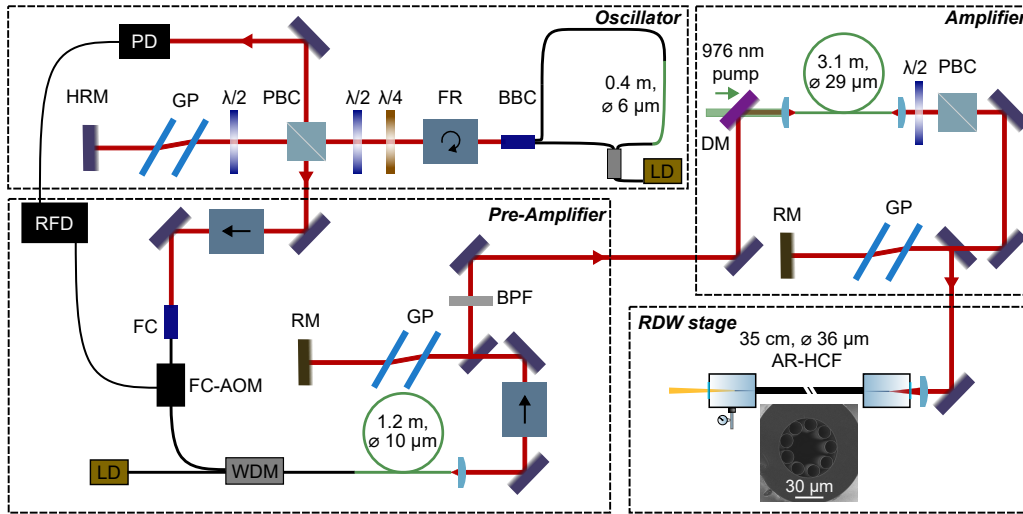


**Fig. 1.** Experimental setup. LD: laser diode; WDM: wavelength division multiplexer; BBC: birefringent beam combiner; FR: Faraday rotator;  $\lambda/2$ ,  $\lambda/4$ : waveplates; PBC: polarizing beam cube; GP: grating pair; HRM: high reflection mirror; PD: photodiode; RFD: radio frequency driver; ISO: isolator; FC: fiber collimator; FC-AOM: fiber-coupled acoustic optic modulator; RM: roof mirror; BPF: bandpass filter; DM: dichroic mirror. The cross-section scanning electron microscope image of the antiresonant hollow-core fiber is shown in the RDW stage.

infrared, that is compact, efficient, and produces coherent, sub-20 fs pulses with significant energy (up to 39 nJ)—corresponding to more than 2.2 MW peak power—at 4.8 MHz, with a simple architecture.

The experimental setup is shown in Figure 1. It consists of an oscillator, a pre-amplification stage, the GMNA stage, and the RDW generation stage. The oscillator is a home-built all-polarization-maintaining mode-locked Yb fiber laser based on a nonlinear amplifying loop mirror (NALM) [27, 28]. The NALM oscillator design was chosen for its simplicity, reliable mode-locking, and environmental stability, achieved through the use of polarization-maintaining fibers. Its Sagnac loop-based artificial saturable absorber also offers long-term stability by avoiding the degradation inherent to physical saturable absorbers. The oscillator is modelocked by increasing the laser pump-diode current above the modelocking current threshold. Once modelocking is achieved, the pump-diode current is lowered to maintain a stable and fundamental modelocking state. The oscillator operates at 48 MHz and generates 0.36 nJ pulses. The output pulse duration is 6.7 ps and can be compressed with an external grating pair to 215 fs. The main output of the oscillator is coupled to a fiber-coupled acoustic-optic modulator. The other output is sent to a photodiode that is connected to a radio-frequency driver to trigger the acoustic-optic modulator. The repetition rate of the oscillator is reduced to 4.8 MHz. The pulses are then amplified in a 10  $\mu\text{m}$  core diameter, 1.2 m long Yb gain fiber that is cladding-pumped at 976 nm. The pre-amplifier output pulses are compressed and filtered to 2.2 nm at full-width half-maximum (FWHM) to have around 1 ps duration and 0.3 nJ energy.

The GMNA stage consists of a 3.1 m long Yb-doped single-mode polarizing large-mode-area photonic crystal fiber with 31  $\mu\text{m}$  mode-field diameter (NKT Photonics). The fiber has a  $\sim 10\text{ dB m}^{-1}$  multi-mode pump absorption at 976 nm. In the GMNA regime, a sub-ps pulse with relatively low energy can be amplified to many hundreds of nJ with sub-40 fs pulse duration [22]. The working principle of a GMNA is the interplay between self-phase modulation and intra-pulse pumping and amplification within the gain band of the fiber, resulting in a longitudinally varying gain profile. This results in a broadband pulse with near-perfect monotonic chirp and a few-ps pulse duration, which can be simply compressed to sub-40 fs with a grating pair. After the GMNA fiber, an achromatic half-waveplate combined with a polar-

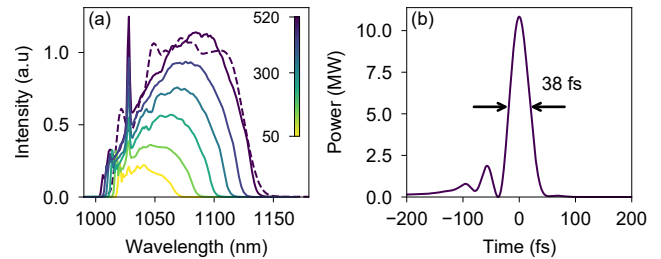


**Fig. 2.** (a) The evolution of GMNA output spectrum as the output pulse energy increases. The inset colorbar indicates the corresponding output pulse energy (nJ). (b) Retrieved temporal profile of the compressed GMNA at the maximum output energy. The dashed line in (a) shows the corresponding retrieved spectrum.

izing beam splitter is employed to control the GMNA energy directed to the next stage. The output pulses are subsequently compressed using a 1000 line/mm grating pair.

The RDW generation stage consists of a 35 cm long antiresonant hollow-core fiber with nine resonators, a core diameter of 36  $\mu\text{m}$ , and a core-wall thickness of 150 nm. According to the antiresonance model [29, 30], both the pump spectrum, spanning 1010 nm to 1140 nm (see Figure 2(a)), and the near-infrared and visible spectral region extending down to 370 nm, are located within the fundamental guidance band. This increases the conversion efficiency from the pump to the RDW, as it avoids crossing a high-loss resonance region. The antiresonant fiber is sealed between two gas cells, with optical access provided by two 3 mm thick uncoated fused-silica windows. At the entrance of the hollow-core fiber, 350 nJ of pulse energy is available. We coupled into the fundamental mode and achieved up to 87% coupling efficiency.

Figure 2(a) presents the experimental amplifier output spectrum with increasing output pulse energy. The maximum pulse energy obtained before observing spectral instability was approximately 520 nJ, with a spectral bandwidth of around 122 nm at  $1/e^2$  of the peak. As the pulse energy increases, the pulse spectral moment shifts to longer wavelengths. This behavior is consistent with the GMNA dynamics,

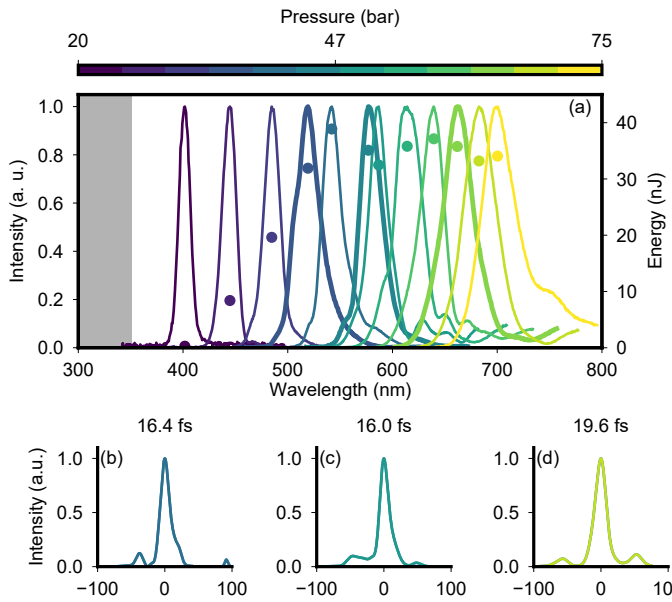


**Fig. 3.** (a) Tunable RDW generation (left axis) in a 36  $\mu\text{m}$  core diameter antiresonant fiber as the argon filling pressure is varied from 20 to 75 bar. The scattered dots (right axis) represent the energy of the corresponding RDWs at the fiber output. The gray shaded area indicates the fiber's first high-loss resonance band. (b)-(d) Retrieved temporal pulse profiles corresponding to the bold spectra in (a), plotted with the same colors.

where the lower pump power towards the end of the fiber causes the blue part of the pulse spectrum to pump the red part, resulting in an overall redshift of the spectrum [22]. We hypothesize that the spectral spike around 1030 nm is due to amplified spontaneous emission from the unconverted pump power, particularly at the fiber input where only a small fraction of the absorbed pump power is extracted by the seed [24]. The experimental output spectrum is collected using an integrated sphere connected to a fiber-coupled CCD spectrometer. The spectrometer covers the spectral range 200 nm to 1200 nm. The whole system is calibrated on an absolute scale with NIST traceable lamps.

To characterize the temporal profile of the GMNA output pulse, we employed an all-reflection second-harmonic generation frequency-resolved optical gating (SHG-FROG). Figure 2(b) shows the retrieved pulse temporal profile with a duration of 38 fs at FWHM. With more than 75% of the pulse energy concentrated in the main pulse, the peak power reaches approximately 10 MW. The retrieved spectrum is presented in Figure 2(a) as a dashed line showing a good agreement with the measured spectra. This pulse duration is comparable to that achievable with Ti:sapphire amplifiers and is sufficiently short to drive RDW generation directly.

Figure 3 shows the generated RDW spectrum from around 400 nm to 700 nm, obtained by varying the argon filling pressure from 20 to 75 bar to tune the phase-matching condition for the RDW [9]. Further tuning beyond 700 nm was also achieved at higher pressures. The RDW energy is represented by the scattered points. These energies were extracted from the calibrated spectra and validated using a power meter and long-pass filter. The RDW energy peaks at around 540 nm with a pulse energy of 39 nJ, resulting in a conversion efficiency of approximately 13% from the coupled energy. This high conversion efficiency is attributed to the absence of a high-loss resonance band in the fiber's transmission spectrum between the pump wavelength and the RDW wavelength. The gradual drop in RDW energy below 500 nm is due to insufficient pump energy (as opposed to interference

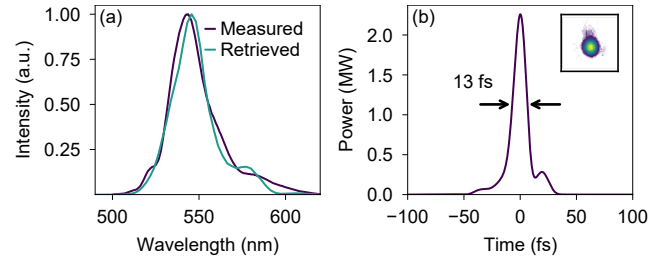


**Fig. 4.** (a) The measured and retrieved spectrum of the RDW pulse generated at 40 bar. (b) Retrieved temporal profile of the pulse SHG-FROG crystal position. The inset in (b) shows the near-field beam profile of the RDW. (c) Retrieved and measured spectrum. (d) Retrieved temporal profile.

from the high-loss resonance band). Shorter wavelength RDW generation occurs at lower gas pressure (and hence lower nonlinearity) and larger frequency shifts from the pump. Both of these reduce the RDW conversion efficiency.

We conducted experiments with the system running for tens of hours without observing any degradation in either amplifier or hollow-core fiber performance.

At the generation point, the RDW pulse is close to its transform-limited duration [31]. However, due to further propagation inside the fiber, output window, collimating lens, and air path, the RDW pulse temporally broadens. To compress the RDW, we first spectrally filter the RDW from the rest of the spectrum using an 850 nm long-pass filter. We then send the RDW to a set of chirped mirrors (PC70, Ultrafast Innovations) to compensate for the positive dispersion acquired after the generation point. We characterized the compressed RDW pulses using an all-reflection SHG-FROG. The crystal used is a type-I 10  $\mu\text{m}$ -thick  $\beta$ -barium borate (BBO) crystal. Figure 4(a) and (b) show the measured and retrieved FROG traces respectively. A good agreement is obtained between the traces, with only 0.8% error between them for a  $512 \times 40$  grid size. Figure 4(d) shows the retrieved temporal profile for the pulse with a pulse duration of 13 fs (FWHM), with more than 81% of the energy located within the main peak. Figure 4(b) inset shows the near-field beam profile for the RDW of the characterized pulse in the same figure, demonstrating a fundamental mode profile. Although much shorter RDW pulses have been obtained previously in antiresonant fibers [15, 31], the limiting factor here is the RDW bandwidth, which increases as the RDW is shifted further from the pump frequency. For example, in Ref. [31], the RDW frequency shift from the pump wavelength is around 750 THz, while for Figure 4 it is only around 200 THz. We also characterized the pulse duration at 65 bar, 45 bar, and 30 bar, shown in Figure 3(b)-(d). All of these measurements resulted in a pulse duration of less than 20 fs.

The presented results demonstrate superior performance compared to current state-of-the-art tunable sources in terms of optical performance (duration, tuning range, peak power) and simplicity (cost, compactness). The absence of bulky optical components and the intrinsic flexibility in the layout of fiber systems, means that the footprint of our presented source can be minimized with careful engineering. In addition, further enhancements to the system are possible. The first two stages, namely the oscillator and the pre-amplifier, could be substituted with a single, more powerful oscillator that possesses the desired repetition rate. This modification would simplify the system and enhance its compactness. The employment of a large-mode-area photonic crystal fiber in this study was intended to demonstrate the most energetic RDW we were able to achieve. It is feasible to achieve tunable pulses with reduced—but adequate—energy using a standard step-index gain

fiber [32]. In contrast, by moderately increasing the pump energy (with a more optimized GMNA), further RDW tuning towards the resonance, below 400 nm, would be feasible.

Our approach offers the potential for expanded tunability into the ultraviolet and infrared spectral domains. As we demonstrated in recent work (ref. [18]), deep-ultraviolet RDW generation is achievable with pump energies as low as approximately 20 nJ in the green spectral region, a level readily accessible via SHG of the laser system described here. Moreover, by filling the antiresonant fiber with a Raman active gas, soliton self-frequency redshifting can be achieved [33, 34]. Consequently, by incorporating an SHG stage and utilizing an appropriate set of antiresonant fibers, a single device could generate tunable ultrashort pulses spanning from the deep ultraviolet to the infrared.

In this work, we demonstrated the generation of tunable sub-20 fs pulses from around 400 nm to beyond 700 nm using a fiber oscillator and gain-managed nonlinear amplifier combined with RDW emission in a gas-filled hollow-core fiber. We achieved pulse durations as short as 13 fs with up to 39 nJ of energy and peak powers as high as 2.2 MW. This compact and efficient setup, operating at 4.8 MHz, offers a compelling alternative to traditional ultrafast tunable light sources, providing comparable or superior performance in terms of pulse duration and tunability while significantly reducing complexity, cost, and footprint. This work highlights the potential of GMNA and RDW techniques to create high-performance, low-cost ultrafast laser sources suitable for a wide range of applications beyond laboratory settings.

**Funding.** This work was funded by the United Kingdom's Engineering and Physical Sciences Research Council: Grant agreement EP/T020903/1. JCT is supported by a Chair in Emerging Technology from the Royal Academy of Engineering and by the Institution of Engineering and Technology (IET) through the IET A F Harvey Engineering Research Prize.

**Acknowledgments.** The authors thank Martin Gebhardt, Christian Brahms, William J. Wadsworth, and Jonathan Knight for useful discussions.

**Disclosures.** The authors declare no conflicts of interest.

**Data availability.** Data underlying the results presented in this paper are not publicly available at this time but may be obtained from the authors upon reasonable request.

## REFERENCES

1. W. Denk, J. H. Strickler, and W. W. Webb, *Science* **248**, 73 (1990).
2. M. Maiuri, M. Garavelli, and G. Cerullo, *J. Am. Chem. Soc.* **142**, 3 (2020). PMID: 31800225.
3. N. Kotsina, C. Brahms, S. Jackson, *et al.*, *Chem. Sci.* **13**, 9586 (2022).
4. R. Ell, U. Morgner, F. X. Kärtner, *et al.*, *Opt. Lett.* **26**, 373 (2001).
5. T. Deckert, A. Vanderhaegen, and D. Brida, *Opt. Lett.* **48**, 4496 (2023).
6. R. Mevert, Y. Binhammer, C. M. Dietrich, *et al.*, *Photon. Res.* **9**, 1715 (2021).
7. H. Tu and S. A. Boppart, *Laser & Photonics Rev.* **7**, 628 (2013).
8. N. Y. Joly, J. Nold, W. Chang, *et al.*, *Phys. Rev. Lett.* **106**, 203901 (2011).
9. K. F. Mak, J. C. Travers, P. Hölzer, *et al.*, *Opt. Express* **21**, 10942 (2013).
10. F. Belli, A. Abdolvand, W. Chang, *et al.*, *Optica* **2**, 292 (2015).
11. K. F. Mak, M. Seidel, O. Pronin, *et al.*, *Opt. Lett.* **40**, 1238 (2015).
12. F. Köttig, F. Tani, C. M. Biersach, *et al.*, *Optica* **4**, 1272 (2017).
13. J. C. Travers, T. F. Grigorova, C. Brahms, and F. Belli, *Nat. Photonics* **13**, 547 (2019).
14. M. Erkintalo, Y. Q. Xu, S. G. Murdoch, *et al.*, *Phys. Rev. Lett.* **109**, 223904 (2012).
15. C. Brahms, D. R. Austin, F. Tani, *et al.*, *Opt. Lett.* **44**, 731 (2019).
16. M. Reduzzi, M. Pini, L. Mai, *et al.*, *Opt. Express* **31**, 26854 (2023).
17. J. M. Dudley, G. Genty, and S. Coen, *Rev. Mod. Phys.* **78**, 1135 (2006).
18. M. Sabbah, K. Harrington, L. R. Murphy, *et al.*, *Opt. Lett.* **49**, 3090 (2024).
19. W. Liu, R. Liao, J. Zhao, *et al.*, *Optica* **6**, 194 (2019).
20. P. Reppen, D. Wandt, U. Morgner, *et al.*, *Opt. Lett.* **44**, 5973 (2019).
21. P. Sidorenko and F. Wise, *Opt. Lett.* **45**, 4084 (2020).
22. P. Sidorenko, W. Fu, and F. Wise, *Optica* **6**, 1328 (2019).
23. M. E. Fermann, V. I. Kruglov, B. C. Thomsen, *et al.*, *Phys. Rev. Lett.* **84**, 6010 (2000).
24. D. Tomaszewska-Rolla, R. Lindberg, V. Pasiskevicius, *et al.*, *Sci. Reports* **12**, 404 (2022).
25. B. Ren, C. Li, T. Wang, *et al.*, *Opt. & Laser Technol.* **160**, 109081 (2023).
26. V. Boulanger, M. Olivier, F. Trépanier, *et al.*, *Opt. Lett.* **48**, 2700 (2023).
27. T. Jiang, Y. Cui, P. Lu, *et al.*, *IEEE Photonics Technol. Lett.* **28**, 1786 (2016).
28. A. S. Mayer, W. Grosinger, J. Fellingner, *et al.*, *Opt. Express* **28**, 18946 (2020).
29. N. M. Litchinitser, A. K. Abeeluck, C. Headley, and B. J. Eggleton, *Opt. Lett.* **27**, 1592 (2002).
30. F. Yu and J. Knight, *IEEE J. Sel. Top. Quantum Electron.* **22**, 1 (2016).
31. A. Ermolov, H. Valtna-Lukner, J. Travers, and P. S. Russell, *Opt. Lett.* **41**, 5535 (2016).
32. M. Sabbah, R. Mears, L. Murphy, *et al.*, "Tunable megawatt-scale sub-15 fs visible pulses via dispersive wave emission pumped by a gain managed fiber amplifier," in *Laser Congress 2024 (ASSL, LAC, LS&C)*, (Optica Publishing Group, 2024), p. AW6A.4.
33. F. Tani, J. Lampen, M. Butryn, *et al.*, *Phys. Rev. Appl.* **18**, 064069 (2022).
34. Y.-H. Chen, J. Moses, and F. Wise, *J. Opt. Soc. Am. B* **40**, 796 (2023).